Supporting Information

Ionic liquid surfactant-derived carbon micro/nanostructures toward application for supercapacitors

Weizheng Li[a], Qiang Gao[a], Ming Shen[a,], Bingyu Li[a], Chuanli Ren[b], Jun Yang[c,*]*

Table S1. EDX element composition analysis result of NMHCSs-1.2-55-0.

Element	NMHCSs-1.2-55-0 (wt.%)			NMHCSs-1.2-55-0 (at.%)		
	a	b	c	a	b	c
C	94.04	93.09	91.66	95.14	94.37	93.31
N	3.07	3.46	3.93	2.66	3.01	3.42
O	2.88	3.43	4.39	2.19	2.61	3.35

Table S2. Fluorescence spectral data of solubilized pyrene under different molar concentration of 3-aminophenol.

curve	c(3-aminophenol) / (mmol · L^{-1})	λ_1 /nm	λ_3 /nm	I_1	I_3	I_1/I_3
0	0.00	372.8	383.7	10050	7473	1.345
1	9.16	372.8	383.6	7870	5859	1.343
2	18.33	372.8	383.7	3345	2523	1.326
3	27.49	372.8	383.7	1835	1387	1.323
4	36.65	372.8	383.6	1361	1040	1.308
5	45.82	372.8	383.6	821	639	1.285
6	54.98	372.8	383.6	859	670	1.282
7	64.14	372.8	383.6	645	508	1.270
8	73.31	372.8	383.7	503	402	1.251
9	82.47	372.8	383.6	339	278	1.219
10	91.63	372.8	383.7	325	272	1.195

Table S3. Elemental compositions of C, N, and O, and relative contents of nitrogen species to N 1s in NMHCSs, NMHCSs-b and A-NMHCSs.

Sample	C (at.%)	N (at.%)	O (at.%)	N-6 (%) 398.3eV	N-5(%) 399.8eV	N-Q(%) 401.0eV	N-OX(%) 402.6eV
NMHCSs-1.2-55-6	87.17	6.72	4.48	37.90	10.90	38.40	12.70
NMHCSs-b	90.24	3.14	5.31	28.90	3.10	62.80	5.20
NMHCSs-1.0-55-6	82.08	6.02	8.53	15.27	12.55	60.88	11.30
NMHCSs-0.8-55-6	85.62	5.30	6.94	23.16	14.07	52.38	10.39
NMHCSs-0.6-55-6	83.47	6.85	6.35	22.73	10.91	59.32	7.04
NMHCSs-0.4-50-25	82.16	6.77	8.74	18.46	10.25	60.43	10.86
A-NMHCSs	74.25	2.92	14.07	-	-	-	-

Table S4. Specific capacitances (F g^{-1}) of NMHCSs-based electrodes at different current densities.

Sample	0.2 A g^{-1}	1 A g^{-1}	3 A g^{-1}	5 A g^{-1}	10 A g^{-1}	15 A g^{-1}	20 A g^{-1}
NMHCSs-0.6-55-6	176	157	143	137	126	120	112
NMHCSs-1.2-55-6	184	166	149	145	136	132	128
NMHCSs-1.2-55-0	198	184	164	155	145	137	132
NMHCSs-1.2-95-0	201	187	166	161	151	145	142
NMHCSs-1.2-55-15	176	155	139	132	120	114	104
NMHCSs-0.4-55-15	138	117	101	93	92	75	72
NMHCSs-0.4-50-25	218	203	184	179	171	166	160
NMHCSs-0.4-25-50	211	195	174	165	142	125	105
A-NMHCSs	308	291	263	254	246	238	233

Table S5. Comparison of specific surface area, pore volume and EDLCs specific capacitance for sample A-NMHCSs with previous reported carbon materials.

Samples	S_{BET} (m^2 g^{-1})	Pore volume (cm^3 g^{-1})	Capacitance (F g^{-1})	Current density	Electrolyte	Ref.
A-NMHCSs	1906	1.43	308	0.2 A g^{-1}	6 M KOH	This work
			293	0.5 A g^{-1}		
			291	1 A g^{-1}		
			254	5 A g^{-1}		
			246	10 A g^{-1}		
			233	20 A g^{-1}		
			208	50 A g^{-1}		
			174	100 A g^{-1}		
GWAC	2134	1.01	150	0.25 A g^{-1}	$TEABF_4$	1
PC –Cs/CNTs	804	0.8	102.5	0.5 A g^{-1}	6 M KOH	2
DUT-108	750	0.38	192	0.2 A g^{-1}	1 M NaCl	3
PANI/CNO	18	/	196	1 A g^{-1}	1 M H_2SO_4	4
FL-CNSs	779	/	60.5	0.05 V s^{-1}	1 M TEABF4	5
SPHA-ac-700–2	1900	1.15	271	1 A g^{-1}	6 M KOH	6
3D-MCA	1750	/	148.6	5 mV s^{-1}	0.5 M TEABF4	7
CBC-800	861	0.861	233.5	0.2 A g^{-1}	6 M KOH	8
biomass-derived	/	/	170	0.5 A g^{-1}	1 M H_2SO_4	9

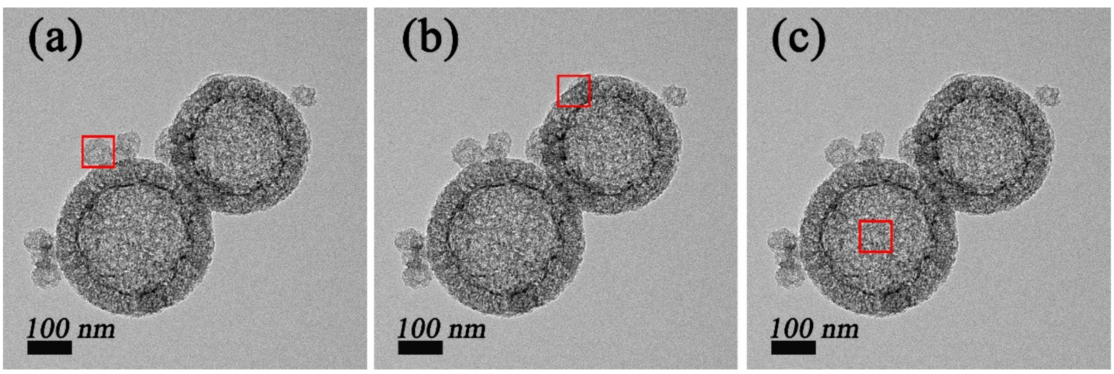

Figure S1. EDX elemental analysis of NMHCSs-1.2-55-0 nanospheres.

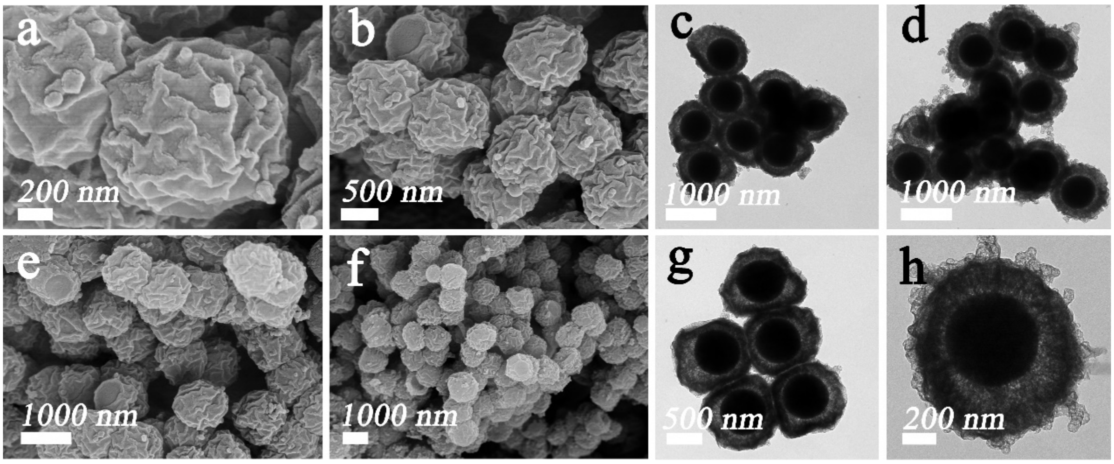

Figure S2. FE-SEM (a, b, e, f) and TEM (c, d, g, h) images of NMHCSs-0.4-55-15 synthesized by nanoemulsion polymerization in the microbalance system of micelles and vesicles.

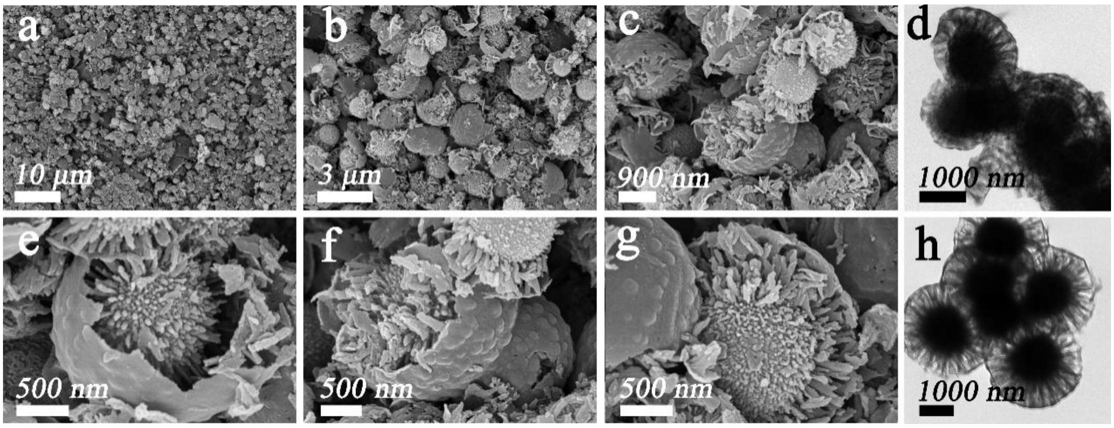

Figure S3. FE-SEM (a, b, c, e, f, g) and TEM (c, h) images of NMHCSs-0.4-50-25 synthesized by nanoemulsion polymerization in the microbalance system of micelles and vesicles.

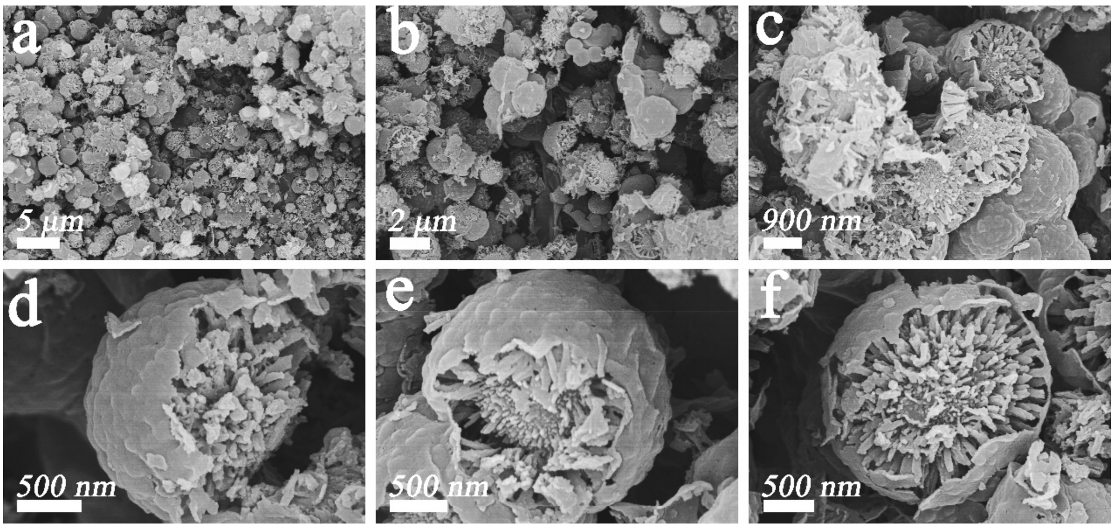

Figure S4. FE-SEM images of open structured hemispheric A-NMHCSs activated by KOH with chrysanthemum-like mesoporous core and ultrathin mesoporous shell.

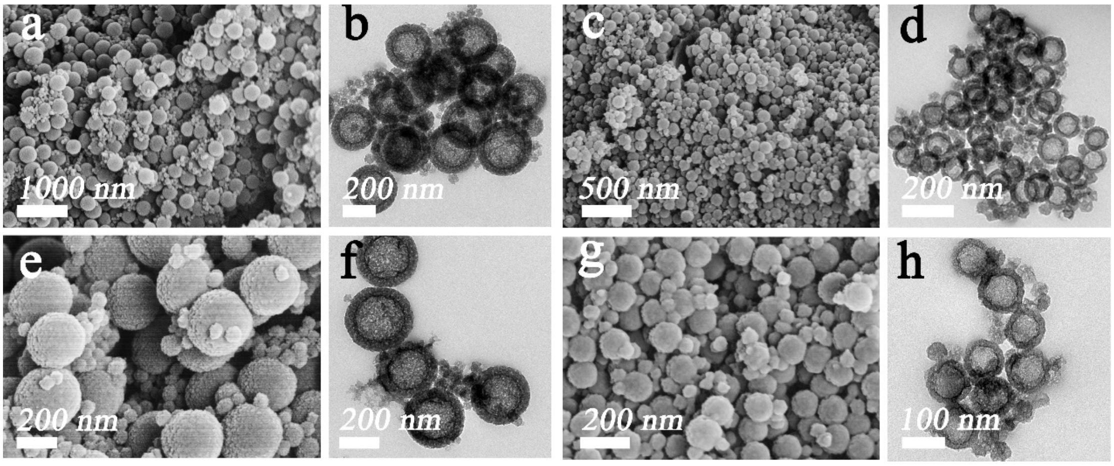

Figure S5. TEM and FE-SEM images of (a, b, e, f) NMHCSs-1.2-55-0 and (c, d, g, h) NMHCSs-1.2-95-0 synthesized by nanoemulsion polymerization in the microbalance system of micelles and vesicles.

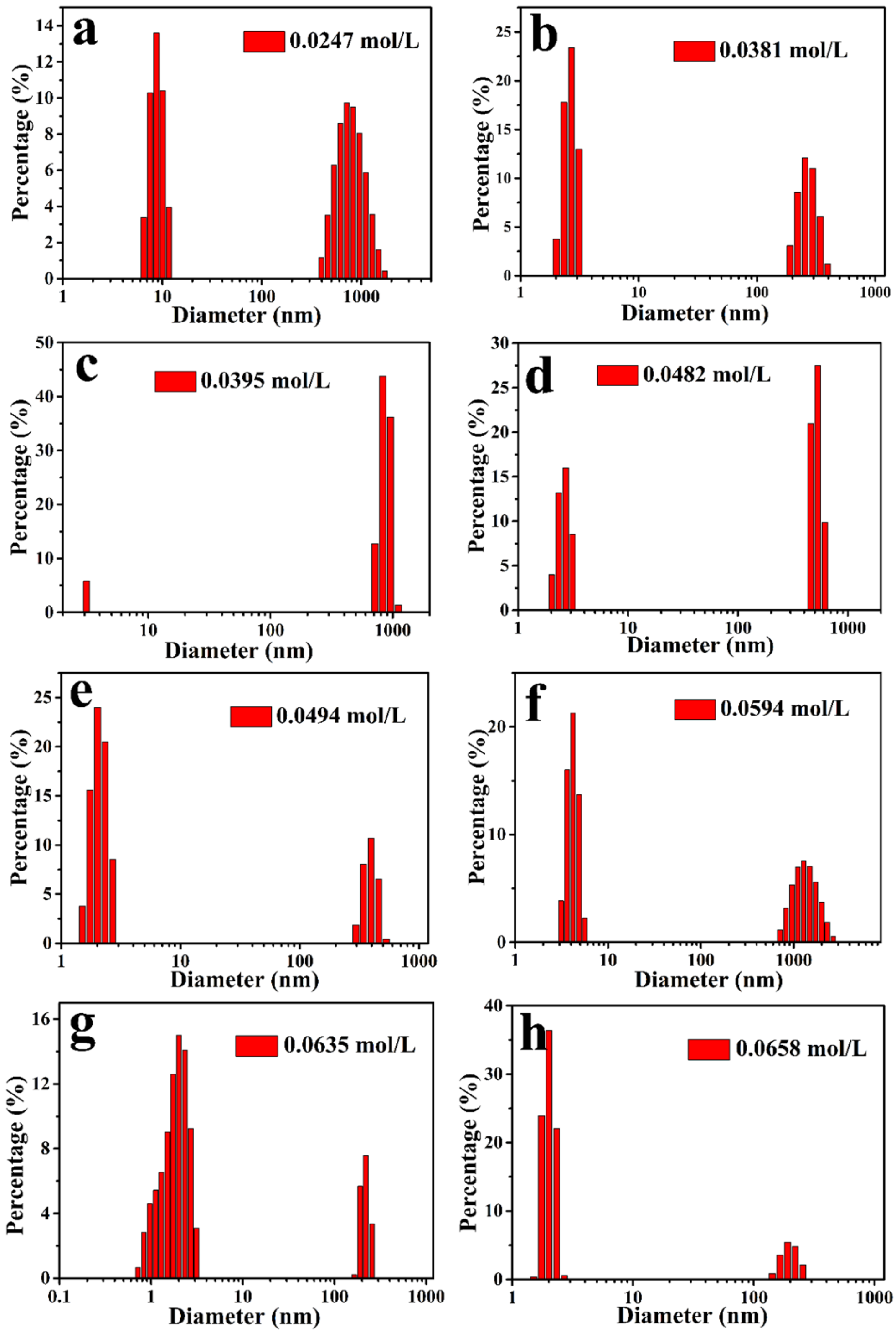

Figure S6. The size distribution for the assemble of ionic liquid surfactant [C_{12}mim]Br with different concentrations in the mixture of water and ethanol obtained by DLS

Figure S7. The photos of the aggregates of $[C_{12}mim]Br$ in the mixture of water and ethanol collected from the reaction systems of the synthesized NMHCSs-1.2-95-0 (a), NMHCSs-1.2-55-0 (b), NMHCSs-1.2-55-6 (c) and NMHCSs-0.4-50-25 (d).

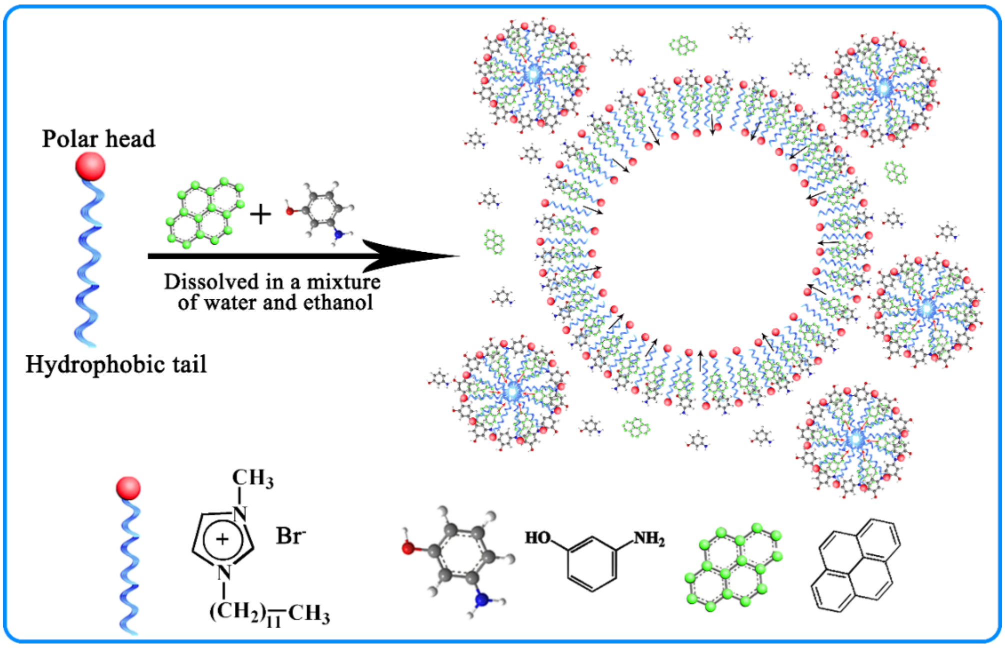

Figure S8. Pyrene fluorescence probe spectrometry characterizes the process of 3-aminophenol compatibilize to the micelles and vesicles of ionic liquid $[C_{12}mim]Br$.

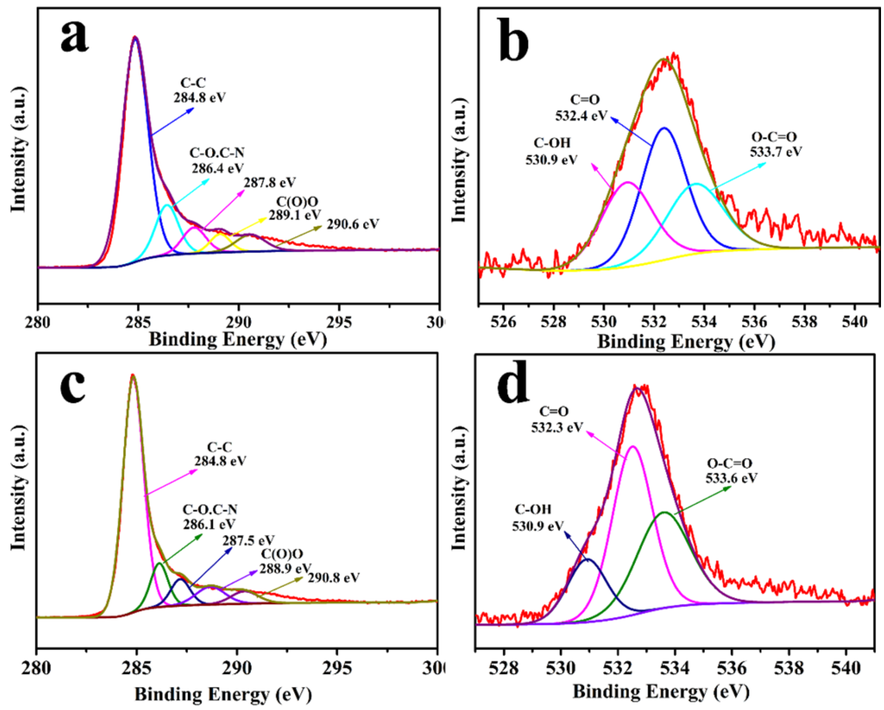

Figure S9. High-resolution spectra of the C 1s, N 1s and O 1s of NMHCSs-1.2-55-6 (a, b) and NMHCSs-b (c, d).

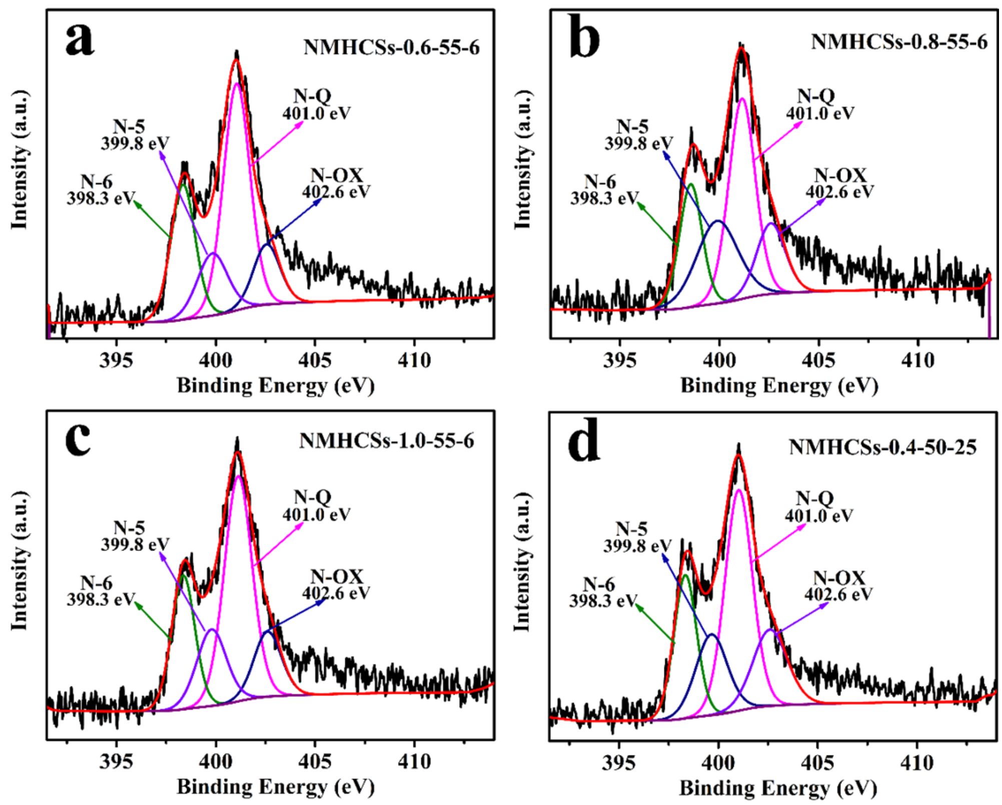

Figure S10. Fitted high-solution XPS spectra of N 1s for NMHCSs-0.6-55-6 (a), NMHCSs-0.8-55-6 (b), NMHCSs-1.0-55-6 (c) and NMHCSs-0.4-50-25 (d).

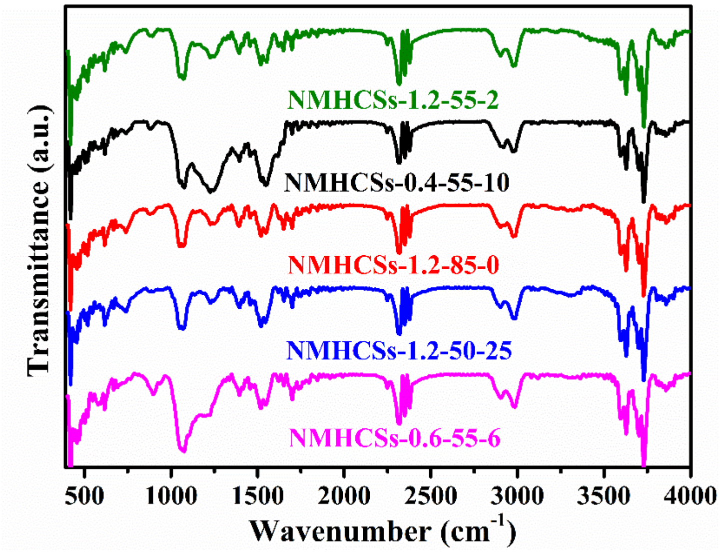

Figure S11. FT-IR spectrums of NMHCSs (NMHCSs-1.2-55-2，NMHCSs-1.2-0.4-55-10，NMHCSs-1.2-85-0，NMHCSs-1.2-50-25 and NMHCSs-0.6-55-6).

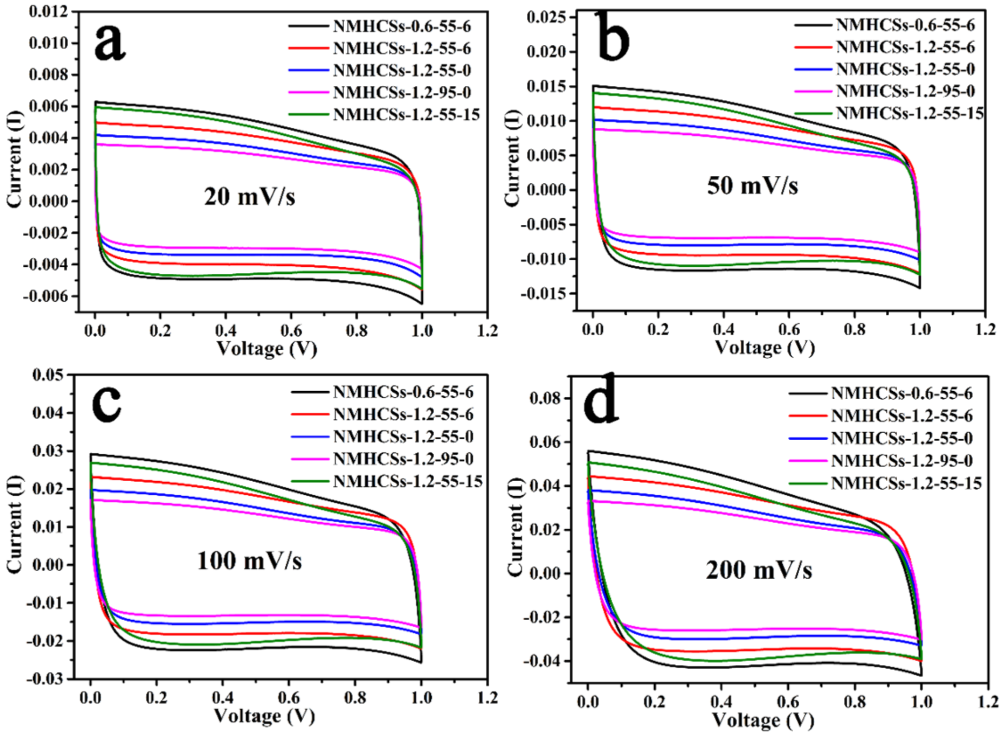

Figure S12. Cyclic voltammograms curves of the prepared NMHCSs (NMHCSs-0.6-55-6, NMHCSs-1.2-55-6, NMHCSs-1.2-55-0, NMHCSs-1.2-95-0 and NMHCSs-1.2-5-15) at the scan rate of 20-200 mV s^{-1}.

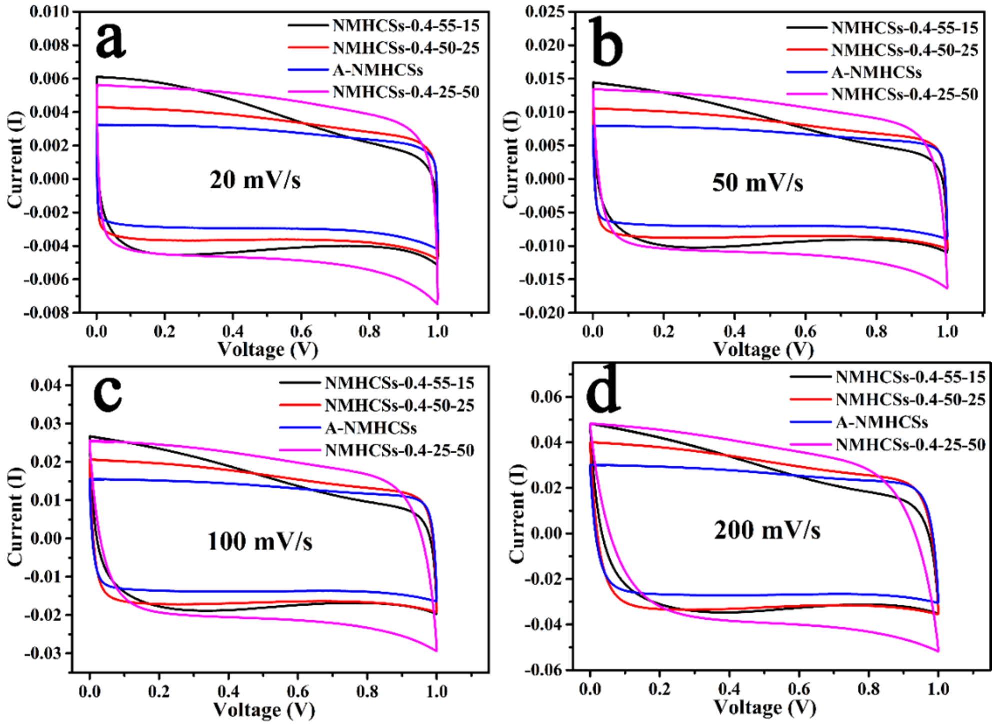

Figure S13. Cyclic voltammograms curves of the prepared NMHCSs (NMHCSs-0.4-55-15, NMHCSs-0.4-50-25, A-NMHCSs and NMHCSs-0.4-25-50) at the scan rate of 20-200 mV s^{-1}.

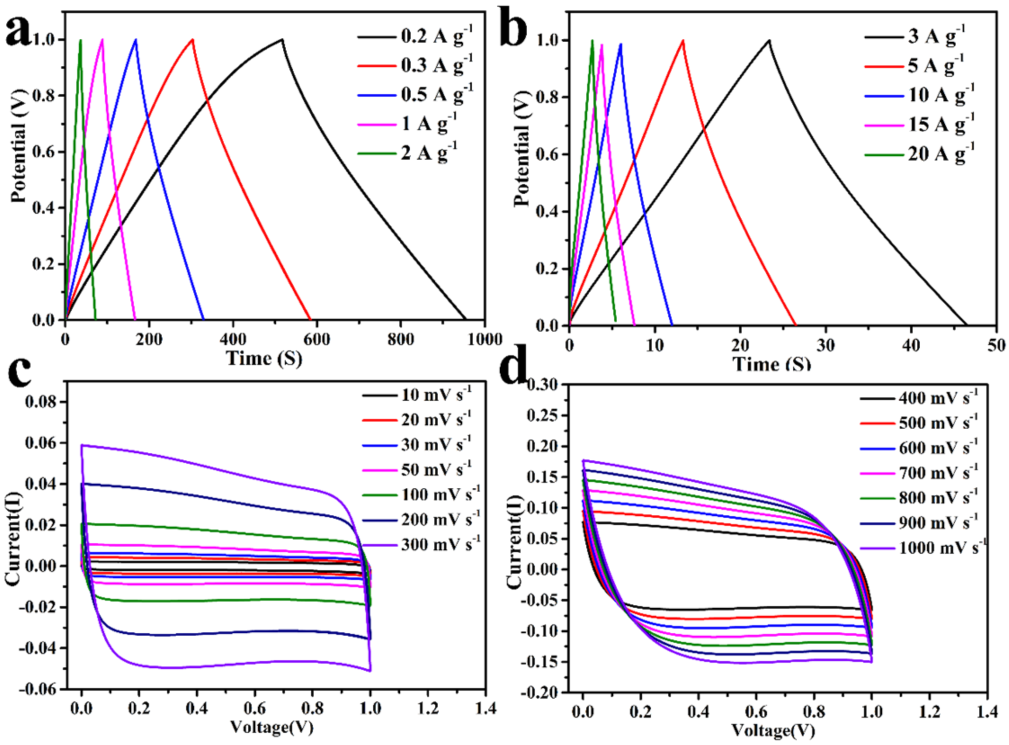

Figure S14. Electrochemical performance of NMHCSs-0.4-50-25 in 6 M KOH electrolyte in a two-electrode system; (a, b) Galvanostatic charge-discharge curves at the current density of 0.2-20 A g^{-1}; (c, d) CV curves at the scan rate of 10-1000 mV s^{-1}.

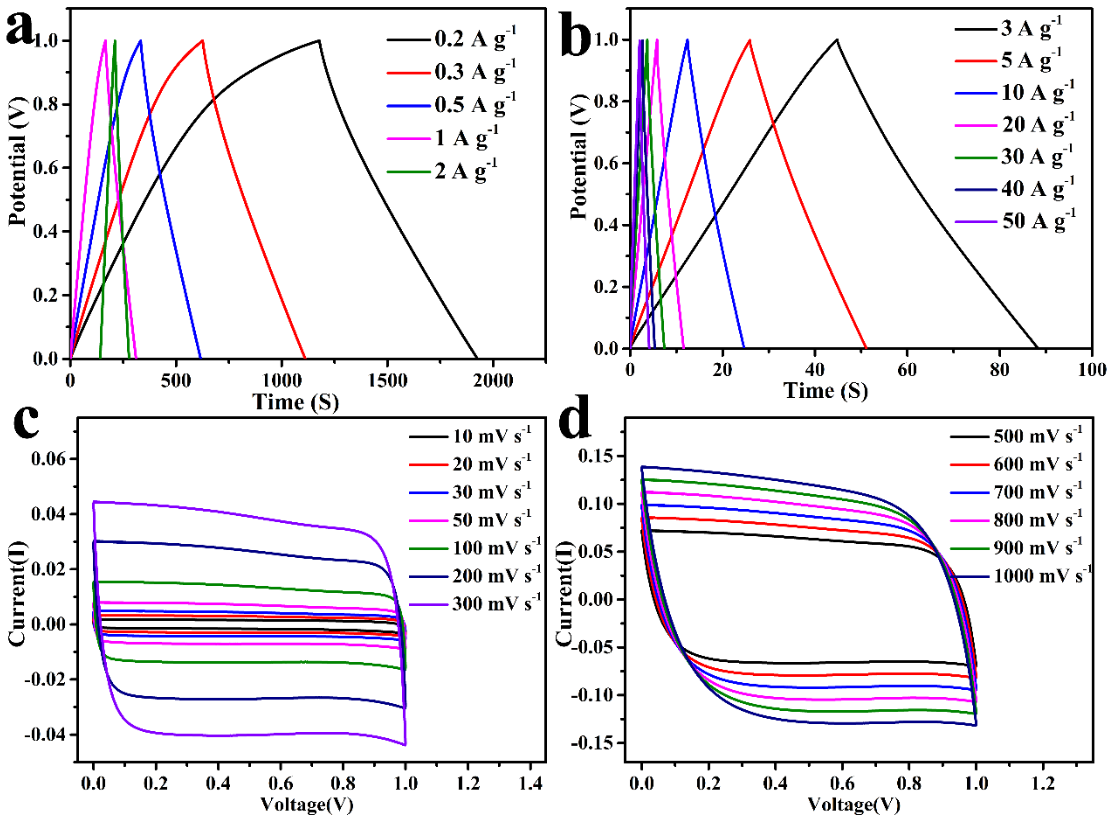

Figure S15. Electrochemical performance of A-NMHCSs in 6 M KOH electrolyte in a two-electrode system; (a, b) Galvanostatic charge-discharge curves at the current density of 0.2-50 A g^{-1}; (c, d) CV curves at the scan rate of 10-1000 mV s^{-1}.

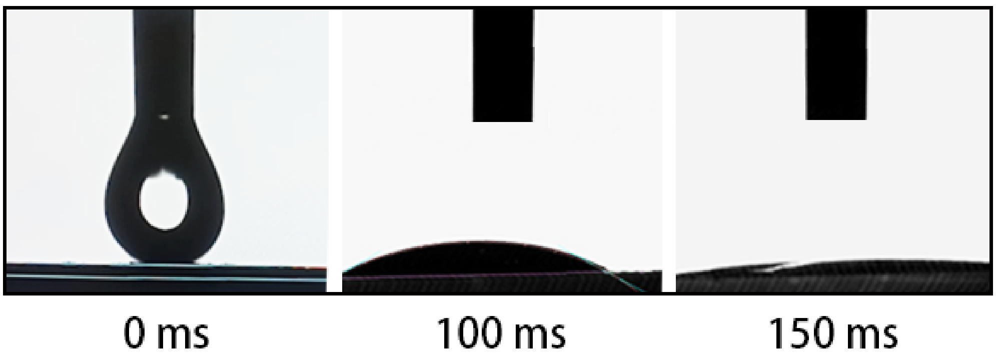

Figure S16. Wettability of electrolyte on the surface of the prepared electrode materials (A-NMHCSs).

Reference:

1 C. Li, X. Zhang, Z. Lv, K. Wang, X. Sun, X. Chen and Y. Ma, *Chem. Eng. J.*, 2021, **414**, 128781.

2 X. Hong, X. Wang, Y. Li, C. Deng and B. Liang, *Electrochim. Acta*, 2021, 139571.

3 C. Huettner, F. Xu, S. Paasch, C. Kensy, Y. X. Zhai, J. Yang, E. Brunner and S. Kaskel, *Carbon*, 2021, **178**, 540–551.

4 M. Majumder, A. K. Thakur, M. Bhushan and D. Mohapatra, *Electrochim. Acta*, 2021, **370**, 137659.

5 M. Zhao, M. Shi, H. Zhou, Z. Zhang, W. Yang, Q. Ma and X. Lu, *Electrochim. Acta*, 2021, **390**, 138783.

6 W. Zhang, B. Liu, M. Yang, Y. Liu, H. Li and P. Liu, *J. Mater. Sci. Technol.*, 2021, **95**, 105–113.

7 B. Yao, H. Peng, H. Zhang, J. Kang, C. Zhu, G. Delgado, D. Byrne, S. Faulkner, M. Freyman, X. Lu, M. A. Worsley, J. Q. Lu and Y. Li, *Nano Lett.*, 2021, **21**, 3731–3737.

8 J. Cui, J. Yin, J. Meng, Y. Liu, M. Liao, T. Wu, M. Dresselhaus, Y. Xie, J. Wu, C. Lu and X. Zhang, *Nano Lett.*, 2021, **21**, 2156–2164.

9 R. Fu, C. Yu, S. Li, J. Yu, Z. Wang, W. Guo, Y. Xie, L. Yang, K. Liu, W. Ren and J. Qiu, *Green Chem.*, 2021, **23**, 3400–3409.